EVALUATION OF MIXING PERFORMANCE OF THREE-DIMENSIONAL JETS USING MATERIAL LINE STRETCHING

Mamoru Takahashi
Department of Mechanical Engineering
Mie University
1577 Kurimamachiya-cho, Tsu-shi, Mie, Japan
takahashi@mach.mie-u.ac.jp

Ryota Matsui
Department of Mechanical Engineering
Mie University
1577 Kurimamachiya-cho, Tsu-shi, Mie, Japan
matsu-r@ees.mach.mie-u.ac.jp

Koichi Tsujimoto
Department of Mechanical Engineering
Mie University
1577 Kurimamachiya-cho, Tsu-shi, Mie, Japan
tujimoto@mach.mie-u.ac.jp

Toshitake Ando
Department of Mechanical Engineering
Mie University
1577 Kurimamachiya-cho, Tsu-shi, Mie, Japan
ando@mach.mie-u.ac.jp

ABSTRACT

We evaluated the mixing performances of three-dimensional turbulent jets using material lines, which are fluid elements convected and stretched by background flows. The material lines were embedded in shear layers of a round jet and a lobed jet with six lobes, having streamwise homogeneity due to periodic boundary conditions. A quantitative comparison of the mixing performances between the round and lobed jets was conducted using statistics derived from the stretched material lines. It was observed that the stretching rate and spatial extent of the material lines in the lobed jet were lower compared to those in the round jet. Material lines initially placed in shear layer regions with small azimuthal curvatures experienced comparable stretching to those in the round jet, whereas those in regions with large curvatures underwent significantly less stretching. However, our discussion suggests that even with the above results, it cannot be conclusively stated that the mixing effect of the lobed jet is necessarily inferior to that of the round jet.

INTRODUCTION

Conventionally, the mixing performance of shear flows, such as jets, has been quantified using the diffusion of the mean velocity or passive scalar fields. However, this method only captures one aspect of mixing effects and is typically static, making it challenging to isolate the contribution of turbulent fields, including coherent structures, solely from the mean field.

Fluid mechanists have sometimes used the deformation of material elements that are passively transported by turbulent flows to study mixing phenomena. When the two fluids are folded in layers in a certain region, we recognize that "the fluid is well mixed. Therefore, evaluating the curvature and fractal dimension of the material elements provides a more intrinsic mixing performance evaluation than mean field diffusion. Since Batchelor (1952), many authors have studied the deformation of material elements due to turbulence numerically (Girimaji & Pope (1990); Goto & Kida (2007)) or experimentally (Guala *et al.* (2005)).
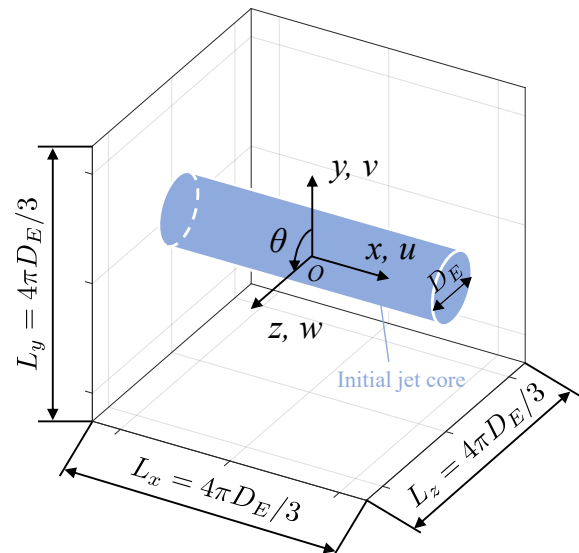

Figure 1. Schematic of numerical simulations.

Most studies on material element deformation have been conducted using homogeneous isotropic turbulence. In this study, we introduced stretching of line-shaped material elements (material lines) to evaluate the mixing performance of a three-dimensional jet. It is widely believed that the mixing performance strongly depends on exit conditions, such as the initial mean velocity profiles and nozzle geometries. Therefore, we investigated the mixing of not only the round jet but also the lobed jet, which is used as a mixing-enhancement device in certain engineering scenarios, to quantify the influence of exit geometry.

NUMERICAL DETAILS
Round and lobed jet flows

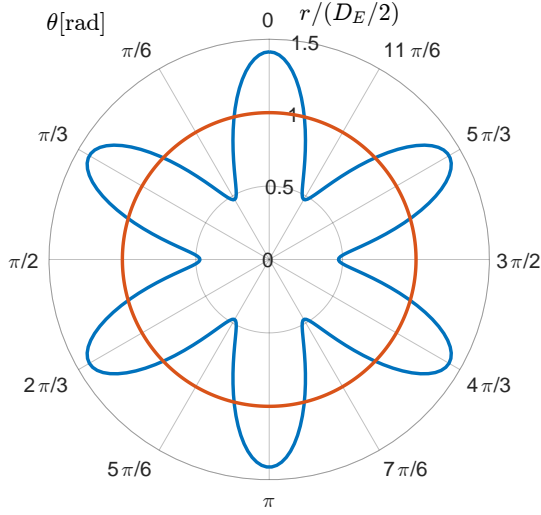Direct numerical simulations of the temporally developing round and lobed jets were conducted. Fig-

Figure 2.　Round (orange) and lobed (blue) geometries.

Figure 3.　Temporal evolution of radial distributions of mean and R.M.S. streamwise velocity of round (top) and lobed (bottom) jets.

ure 1 shows a schematic of the numerical simulations. The numerical domain sizes along the x (streamwise), y (vertical), and z (spanwise) directions were $(L_x, L_y, L_z) = ((4\pi/3)D_E, (4\pi/3)D_E, (4\pi/3)D_E)$, where D_E is the equivalent jet diameter. The number of grid points was $(N_x, N_y, N_z) = (256, 256, 256)$. In this study, the mixing performance of jets in the initial developing states is investigated, and the numerical domain size is required to be large so that the primary roller vortices arising from the Kelvin–Helmholtz instability are adequately reproduced. The current setup is comparable to that in the plane jet simulation by da Silva & Pereira da Silva & Pereira (2008) $(4H, 6H, 4H)$. Periodic boundary conditions were set for all the three directions. In the initial state, columnar high-speed $(u = U_J)$ regions were embedded in the computational domain, and their cross-sectional geometries were round or lobed. The initial jet Reynolds number, Re_J, was $D_E U_J / \nu = 3000$.

The flows follow the Navier-Stokes equations and the continuity equation, normalized by D_E and U_J,

$$\frac{\partial u_i}{\partial t} + u_j \frac{\partial u_i}{\partial x_j} = -\frac{\partial p}{\partial x_i} + \frac{1}{Re_J}\frac{\partial^2 u_i}{\partial x_j \partial x_j} \tag{1}$$

$$\frac{\partial u_i}{\partial x_i} = 0 \tag{2}$$

These equations were solved using a projection method solver that consists of pseudospectral scripts for spatial numerical derivative, a 4th order Runge-Kutta scheme for temporal increment, and de-aliasing using the 2/3 rule.

In this study, we tested two types of jet initial conditions: round geometry and lobed geometry. Figure 2 shows the curves giving the round and lobed geometries. The geometries of the jet exits in this study are determined by the following formation:

$$r(\theta) = \frac{D_E}{2}\sqrt{\frac{2b^2}{2b^2 + 1}\left(1 + \frac{\cos a\theta}{b}\right)} \tag{3}$$

where r is the radial direction from the centre axis and θ is the azimuth ($0 \leq \theta \leq 2\pi$). The exit area is evaluated $\int r(\theta)^2/2\mathrm{d}\theta = \pi D_E^2/4$. The parameter a (an integer) determines the number of lobes, and b (positive real number) controls the curvature of the lobes. The limit of $b \to \infty$ yields a

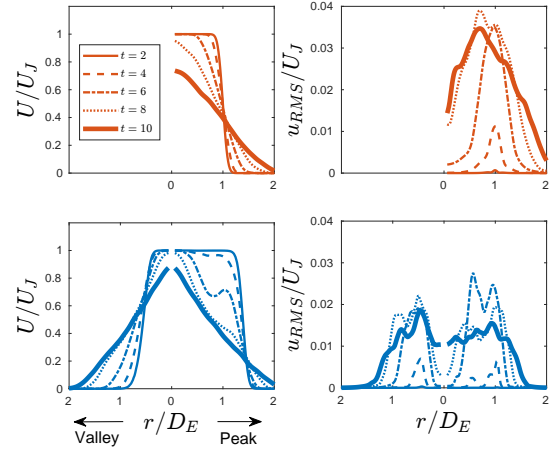round shape whose radius is $D_E/2$. Many studies (Hu *et al.* (2002); Nastase & Meslem (2010); Aleyasin *et al.* (2017)) have investigated lobed jets with six lobes. In this study, the set of $a = 6$ and $b = 2$, which gives geometry similar to that shown in the abovementioned studies, was tested.

Figure 3 shows the temporal evolution of the radial distributions of the mean and R.M.S. streamwise velocities of the round and lobed jets. Averaging is performed in the streamwise and azimuthal directions; thus, the statistics vary with time. For the lobed jet, however, the statistics along the convex and concave directions of the lobed geometry (Peaks and Valleys, respectively, defined later) are separately evaluated. The statistics do not converge well, but this should be resolved by repeating the simulation multiple times and obtaining their ensemble average. The R.M.S. streamwise velocity distributions show that the lobed jet diffuses earlier; therefore, the peak of the distribution is higher for the round jet. This is because the vortex rings in lobed jets with non-uniform axial curvature collapse and break up earlier than those in round jets, resulting in the enhanced diffusion of the turbulent field, which is consistent with the visualization results of the lobed jet field shown in previous studies (Hu *et al.* (2002); Nastase & Meslem (2010)). This study focused on how they contribute to the deformation of passive materials.

Material lines

The material lines consist of passive tracer particles governed by the following equation,

$$\frac{d\mathbf{X(t)}}{dt} = \mathbf{u}(\mathbf{X}(t), t) \tag{4}$$

where $\mathbf{X}$ and $\mathbf{u}$ are the instantaneous locations and velocities of the particles, respectively. The equation was integrated using the 4th-order Runge Kutta scheme. The velocities of the particles were determined via linear interpolation from the velocity field on the numerical grid.

At each time step, if the distance between two adjacent particles exceeds half of the grid spacing, a new particle is inserted between them, and the line is reconnected. Due to the periodic nature of the jet flows in the streamwise direction, even if a particle is transported out of the numerical domain, an extended velocity field can be reconstructed by connecting the
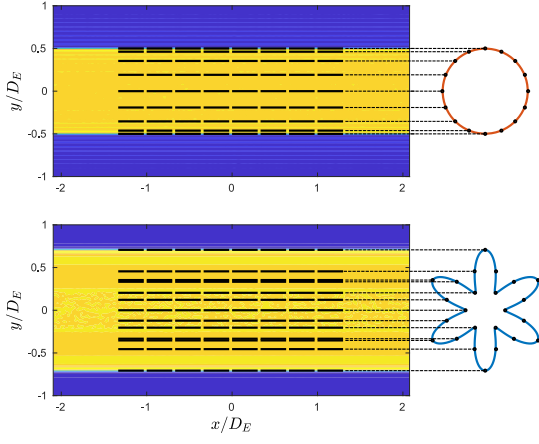
Figure 4. Initial arrangement of material lines in round and lobed jets. The background color shows the initial instantaneous streamwise velocity distribution over $x - y$ plane at $z = 0$.
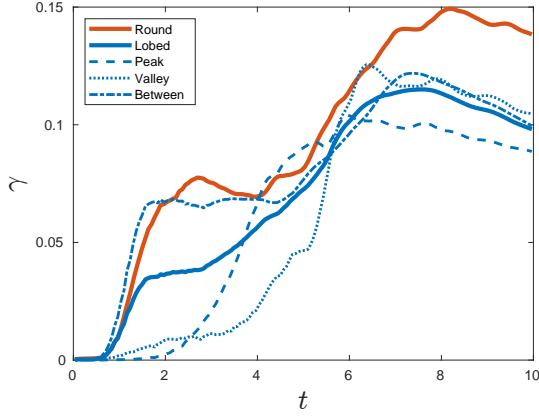

Figure 5. Temporal evolution of statistical stretching rate of material lines.

Figure 6. Temporal evolution of statistical spatial extent of material lines.

The individual stretching rate γ is given as,

$$\gamma \equiv \frac{d}{dt} \log L(t), \qquad (5)$$

where $L(t)$ is the length of each line at $t = t$. In $t \lesssim 1.0$, the γs of the round and lobed jets are comparable. In $t \gtrsim 1.0$, however, the γ of the round jet is always larger than that of the lobed jet. The three thin dashed, dotted, and dot-dashed lines indicate the γs at the Peaks, Valleys, and Middles of the lobed jet, respectively. In $t \lesssim 6.0$, the γ of the Middle is comparable to that of the round jet. Meanwhile, the γs of the Peak and Valley evolve at $t \gtrsim 2.0$ and $t \gtrsim 4.0$, respectively, which are later than those in the round jet and at the Middle. In $t \gtrsim 6.0$, all results of the lobed jet are significantly smaller than that of the round jet. From these results, one might conclude the inferior mixing performance of the lobed to the round jets in these states.

Figure 6 shows the temporal evolution of statistical spatial extent of material lines. The individual spatial extent Δ is given as,

$$\Delta \equiv \sqrt{\frac{1}{L} \int_L (\mathbf{X}_p(s) - \mathbf{X}_G)^2 ds}, \qquad (6)$$

where $\mathbf{X}_p(s)$ is the location of the line element ds, $\mathbf{X}_G$ is the center of gravity of the material line and s is the arc length. While γ is expected to reflect the elongation due to small-scale structures, Δ represents the macroscopic transport by large-scale structures. It is interesting, however, that the relationship between γ and Δ is roughly consistent over time. Similar to γ, the Δ of the Middle of the lobed jet was comparable to that of the round jet and greater than those of the Peak and Valley of the lobed jet. In particular, Δ of the line in the Valleys starts to grow slowly and hardly changes until $t \sim 6$.

From Batchelor (1952), the passive vector e_i evolves according to the following equation.

$$\frac{de_i}{dt} = A_{ij} e_j, \qquad (7)$$

where $A_{ij} \equiv \partial u_i / \partial x_j$ is the velocity gradient tensor. Figure 7 shows the streamwise mean of A_{ij}^2 at $t = 2, 4$, and 6. Note that, the results of the round jet are shown in the upper panel and

numerical domain with its replica. Other particle properties include the neglect of inter-particle interference, disregard for inertial forces, and infinitesimal volume to ensure no impact on the flow field evolution.

As shown in Fig. 4, the initial placement of the material lines was made at eight locations on the shear layer of the jet, parallel and equally spaced in the direction of the main flow. The azimuthal positions were equidistant and were placed every $\pi/8$ for the round jet and $\pi/12$ for the lobed jet. Therefore, the numbers of material lines were set to 128 and 192 for round and lobed jets, respectively. The initial length of the material line was set to $D_E/3$ and consisted of 50 particles. Furthermore, in a lobed jet, the convex parts of the geometry are referred to as "Peaks," the concave parts as "Valleys," and the intermediate positions between them as "Middles." The statistics of the material lines were treated differently according to the position of the lines at the initial time.

Results and discussions

Figure 5 shows the temporal evolution of the statistical stretching rate of material lines in the round and lobed jets.
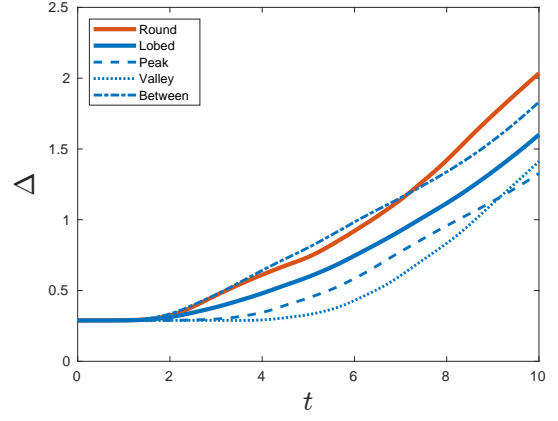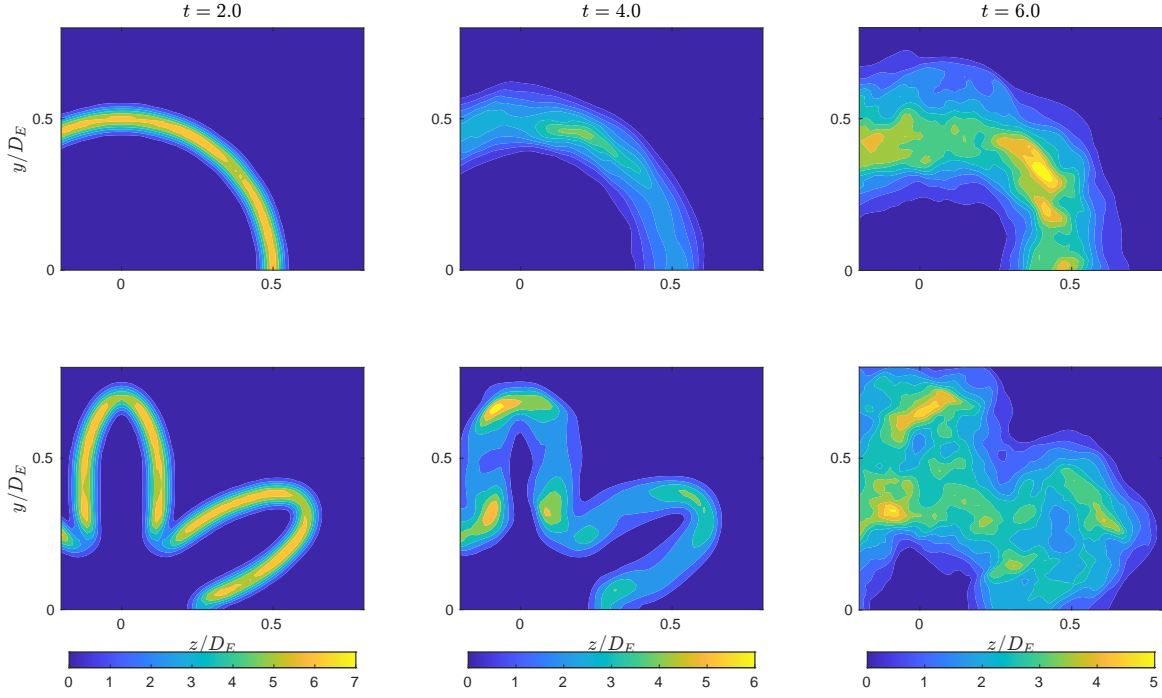
Figure 7.   Temporal evolution of streamwise-averaged A_{ij}^2 in round (top) and lobed (bottom) jets.
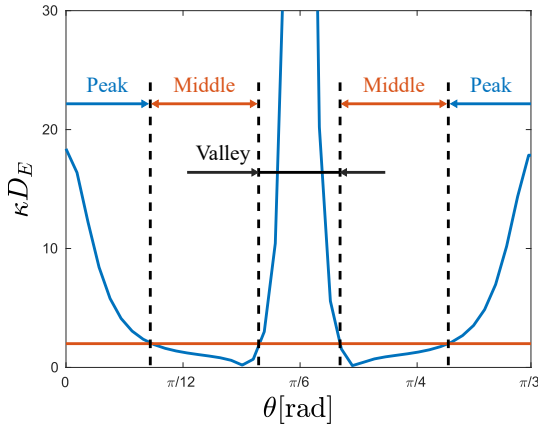

Figure 8.   Curvature of round (red) and lobed (blue) exits along $0 \le \theta \le \pi/3$.
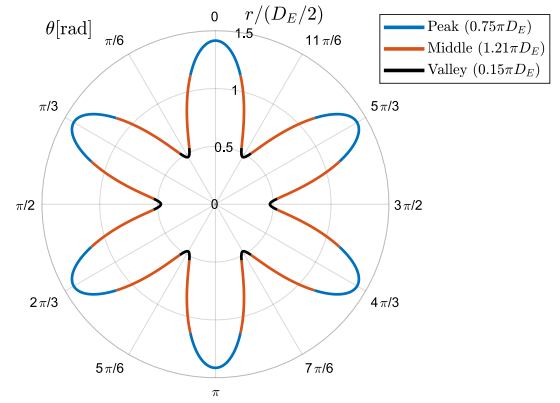

Figure 9.   Distribution of the Peak, Valley, and Middle parts in the lobed geometry.

those of the lobed jet in the lower panel, and the range of colors differs for each time. At $t = 2$, A_{ij}^2 at the Middles of the lobed jets are comparable to those of round jets, with smaller values at Peaks and Valleys compared to them. At $t = 4$, large values are concentrated at Peaks, but relatively small values are observed at Valleys. However, there are large value concentrations on both sides of the Valleys, which diffuse and merge to realize the stretching of the material lines at the Valley in $t \gtrsim 4$. The above is in good agreement with the behaviors of the plots in Figs. 5 and 6.

The above results suggest that the azimuthal curvature of the shear layer is associated with the stretching of the material lines. Specifically, lines located at locations with large azimuthal curvature tend to experience less stretching than others. Note that the impact of whether the shear layer is convex or concave is not clear at the current stage. In our current setup, there are eight material lines at the Peaks, Valleys, and Middles of the lobed jet, with each set accounting for 25% at Peaks and Valleys, and 50% at the Middle. Therefore, the results in

Figs. 5 and 6 could be interpreted as suggesting that the overall mixing performance of the lobed jet is inferior to that of the round jet.

Therefore, lobed geometries are more precisely classified into Peaks, Valleys, and Middles based on their azimuthal curvature. Here, the parts where the curvature is less than or equal to that of the round geometry are defined as Middles, the convex parts with larger curvature are Peaks, and the concaves are Valleys. The curvature distribution of the round and lobed geometry in the azimuthal direction is shown in Fig 8. Furthermore, Fig 9 shows the distribution of the Peaks, Valleys, and Middles over the lobed geometry, along with their respective arc lengths. From Figs 8 and 9, it can be seen that the sum of the arc length of the Middles alone exceeds the entire circumference of the round geometry. Since the stretching of the material lines is considered as the mixing performance per unit azimuthal length, it can be understood that the mixing of the lobed jet is not inferior to that of a round jet when arc lengths are taken into account. In addition, the lines are less stretched at Peaks and Valleys, and the current γ and Δ averages those

4

with Middle, underestimating the overall results of the lobed jet. It should be noted that in actual mixing, the stretching in each part of the geometry is not averaged, but rather is added up to give the final mixing results. Therefore, it does not act to suppress the (not bad) mixing performance in the Middle.

Conclusions

In this study, DNSs of temporally developing round and lobed jets at Reynolds number of 3000 were conducted, and the stretching phenomena induced by these two jet fields on material lines were investigated. The statistical characteristics of the material lines were used to determine the mixing performance of the round and lobed jets in their initial developing states. The material lines were initially oriented in the streamwise direction in the shear layers of the jets with constant spacing in the azimuthal direction.

The stretching rate and spatial extent of the material lines indicate that, at any azimuthal location within the shear layer, the deformation of the material lines in the lobed jet is smaller compared to that in the round counterpart. Material lines situated in shear layer regions with small azimuthal curvatures experience comparable stretching to those in the round jet, whereas those in regions with large curvatures undergo significantly less stretching. Moreover, lines positioned in the Valleys, i.e., the concave regions of the lobed geometry, exhibit the poorest stretching performance. Furthermore, following the equation governing the evolution of the passive vector element, the stretching performance of the lines aligns well with the distribution of the squared sum of the velocity gradient in the shear layers.

However, these results do not directly lead to the conclusion that the mixing performance of the lobed jet is inferior to that of the round jet. It should be noted that the arc length of the lobed geometry exceeds that of the round jet. If the initial positions of the material lines were equispaced along the curves of the geometry, one would conclude that the mixing performance of the lobed jet is superior to that of the round jet. While investigation of material surface stretching instead of lines was not conducted in this study due to the substantial computational resources required, it could address this issue. Moreover, it is worth noting that the current quantification techniques and resulting considerations are applicable not only to discussing the mixing performance of lobed jets but also to that of any other non-circular jets.

REFERENCES

Aleyasin, Seyed Sobhan, Tachie, Mark Francis & Koupriyanov, Mikhail 2017 PIV measurements in the near and intermediate field regions of jets issuing from eight different nozzle geometries. *Flow, Turbulence and Combustion* **99** (2), 329–351.

Batchelor, G K 1952 The effect of homogeneous turbulence on material lines and surfaces. *Proceedings of the Royal Society of London. Series A, Mathematical and physical sciences* **213** (1114), 349–366.

Girimaji, S S & Pope, S B 1990 Material-element deformation in isotropic turbulence. *Journal of fluid mechanics* **220**, 427–458.

Goto, Susumu & Kida, Shigeo 2007 Reynolds-number dependence of line and surface stretching in turbulence: folding effects. *Journal of fluid mechanics* **586**, 59–81.

Guala, Michele, Lüthi, Beat, Liberzon, Alexander, Tsinober, Arkady & Kinzelbach, Wolfgang 2005 On the evolution of material lines and vorticity in homogeneous turbulence. *Journal of fluid mechanics* **533**, 339–359.

Hu, H, Saga, T, Kobayashi, T & Taniguchi, N 2002 Mixing process in a lobed jet flow. *AIAA journal* **40**, 1339–1345.

Nastase, Ilinca & Meslem, Amina 2010 Vortex dynamics and mass entrainment in turbulent lobed jets with and without lobe deflection angles. *Experiments in fluids* **48** (4), 693–714.

da Silva, Carlos B & Pereira, José C F 2008 Invariants of the velocity-gradient, rate-of-strain, and rate-of-rotation tensors across the turbulent/nonturbulent interface in jets. *Physics of fluids* **20** (5), 055101.